GEOPHYSICS, VOL. 60, NO. 6 (NOVEMBER-DECEMBER 1995); P. 1691–1697, 6 FIGS.

Efficient computation of apparent resistivity curves for depth profiling of a layered earth

Umesh C. Das* and Adrianus T. de Hoop‡

ABSTRACT

The problem of computing the electrical potential as a result of a direct current electric source in a layered earth is reformulated to avoid instability in the numerical computation that may occur with the standard propagator matrix formalism described in a number of textbooks. The present spectral formalism involves constituents that contain only exponential functions with nonpositive arguments. The vertical spectral input admittances at the interface levels up to the source level are calculated recursively, starting at the uppermost and lowermost interfaces of the layered earth. These admittances at the source level are then used to compute the electrical voltage at the source level. With the known voltage and the admittances at the source level, the spectral amplitudes at the source level are known. Computation of the amplitudes at the other interfaces is, progressively, carried out by expressing the amplitudes at any interface above the source level in terms of the amplitude on the interface just below it and expressing the amplitudes at any interface below the source level in terms of the amplitude on the interface just above it. This results in an efficient scheme for computing electrical potential in any arbitrary depth levels (required for imaging subsurface conductivity).

We simulate single-borehole and hole-to-hole experiments. Neglecting the influence of the boreholes, we consider a plane layered earth model in which point electrodes along a vertical line (source line) inject and extract a stationary electric current, and point electrodes either along the source line or along another vertical line (receiver line) measure a potential difference. From the potential measurements, apparent resistivities are computed along the vertical lines.

INTRODUCTION

The propagator matrix formalism has been extensively used in the geophysical modeling of a layered earth (Gilbert and Backus, 1966; Fahmy and Adler, 1973; Bhattacharya and Patra, 1968; Koefoed 1979; Kaufman and Keller, 1983). In this formalism, the field quantities at two different levels are expressed in terms of each other via a propagator matrix in which exponentials with positive arguments (or hyperbolic functions) occur. This may result in a loss of computational accuracy. When the propagation is carried out from one end (i.e., either from the uppermost or lowermost interface) up to the source level, exponentials with positive argument may be avoided through appropriate mathematical manipulations (Koefoed 1979). However, for a buried source problem, when the propagation has to be carried out beyond the source level, numerical difficulties do occur because of positive exponentials. For example, we refer to the work of Daniels (1978) in which the electrical potential computations, as a result of the buried electrical point current electrodes, are carried out with a recursive scheme in which exponential functions of the form $\exp(\lambda h)$ occur, where the horizontal wavelength λ and the vertical distance h are positive quantities (see Appendix in Daniels, 1978). In such computations, numerical instability arises because of limited computer accuracy. In this paper, we have reformulated the problem of computing the electrical potential caused by a direct current source at an arbitrary depth by using only the exponentials with nonpositive arguments (as used in the scattering matrix formalism, Kennett, 1974). This results in a numerically stable algorithm. Using a Gauss-Laguerre quadrature method and the method of convolution (Ghosh, 1971), numerical computations are carried out to produce apparent resistivity depth profiles for single-borehole and cross-borehole measurements in layered earth models.

Manuscript received by the Editor September 20, 1993; revised manuscript received February 2, 1995.
*Formerly Technical Geophysics, Delft University of Technology, Delft, The Netherlands; presently, Curtin University of Technology, GPO Box U1987, Perth 6001, Western Australia.
‡Laboratory for Electromagnetic Research, Delft University of Technology, Delft, The Netherlands.

CONFIGURATION

We consider a piece-wise homogeneous, isotropic, plane layered earth model and introduce a circularly cylindrical coordinate system $\{r, \theta, z\}$ with the z-axis positive downwards (Figure 1). The configuration consists of an upper half-space $D(0)$ for which $-\infty < z < z(1)$, a stack of $(ND - 1)$ layers, $\{D(ID);\ ID = 1, \ldots, ND - 1\}$, for which $z(ID) < z < z(ID + 1)$ and a lower half-space $D(ND)$ for which $z(ND) < z < \infty$. The conductivity of $D(ID)$ is $\sigma(ID)\{ID = 0, \ldots, ND\}$. In the horizontally layered earth, we shall compute the apparent resistivity curves for a typical single vertical borehole setting and a typical vertical, cross-borehole electrical sounding configuration. The influence of the boreholes is neglected. Two point electrodes that move along a vertical line (source line) inject and extract a stationary electric current, and two other point electrodes that move either along the same line (thus, simulating a single-borehole experiment) or along another vertical line (receiver line, thus simulating a cross-borehole experiment) measure a potential difference. The aim is to reconstruct from the measurements the vertical distribution of the resistivities (or conductivities) in the different layers. The z-axis is taken along the source line. The electric potential V is then rotationally symmetric around the source line, i.e.,

$$V = V(r, z). \tag{1}$$

The vertical component of the volume density of electric current J_z is then

$$J_z = -\sigma \partial_z V, \tag{2}$$

where ∂_z denotes differentiation with respect to z. We represent $V(r, z)$ as the inverse Fourier-Bessel integral

$$V(r, z) = \frac{1}{2\pi} \int_0^\infty \tilde{V}(\lambda, z) J_0(\lambda r) \lambda \, d\lambda, \tag{3}$$

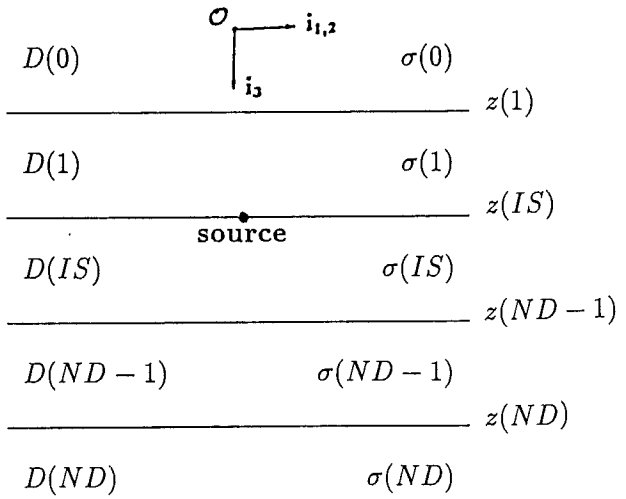

FIG. 1. A layered earth with a buried point source. Each layer is a domain $D(ID)$, $\{ID = 0, \ldots, ND\}$. Two adjacent domains $D(ID)$ and $D(ID + 1)$ are separated by interface $z(ID + 1)$.

in which, in any homogeneous and source-free domain, $\tilde{V} = \tilde{V}(\lambda, z)$ has to satisfy the following differential equation:

$$\partial_z^2 \tilde{V} - \lambda^2 \tilde{V} = 0. \tag{4}$$

In equation (3), J_0 is the Bessel function of the first kind and order zero. The expressions for $\tilde{V}$, and correspondingly for $\tilde{J}_z$ [cf. equation (2)], in a domain $D(ID)$ are given by (omitting the variable λ and including the domain indication ID in the argument list of $\tilde{V}$)

$$\tilde{V}(ID, z) = A^+(ID) \exp[-\lambda(z - z(ID))] + A^-(ID) \exp[-\lambda(z(ID + 1) - z)], \tag{5}$$

$$\tilde{J}_z(ID, z) = \lambda\sigma(ID)[A^+(ID) \exp[-\lambda(z - z(ID))] - A^-(ID) \exp[-\lambda(z(ID + 1) - z)]] \tag{6}$$

$$\text{for } z(ID) < z < z(ID + 1); \quad ID = 1, \ldots, ND - 1.$$

Besides, with due consideration that in the two outer half-spaces $A^+(0) = 0$ and $A^-(ND) = 0$, we have in the upper half-space,

$$\tilde{V}(0, z) = A^-(0) \exp[-\lambda(z(1) - z)] \quad \text{for } -\infty < z < z(1), \tag{7}$$

$$\tilde{J}_z(0, z) = -\lambda\sigma(0)A^-(0) \exp[-\lambda(z(1) - z)] \quad \text{for } -\infty < z < z(1), \tag{8}$$

and in the lower half-space,

$$\tilde{V}(ND, z) = A^+(ND) \exp[-\lambda(z - z(ND))] \quad \text{for } z(ND) < z < \infty, \tag{9}$$

$$\tilde{J}_z(ND, z) = \lambda\sigma(ND)A^+(ND) \exp[-\lambda(z - z(ND))] \quad \text{for } z(ND) < z < \infty. \tag{10}$$

Note that the exponential functions in the representations have been chosen such that their arguments are nonpositive. In equations (5)–(10), the coefficients A^+ and A^- are to be determined from the jump condition at the source level and the boundary conditions at the interface levels. Using the electrical voltage and the vertical volume density of electric current, we define an input admittance at an arbitrary level z [up to the source level $z(IS)$] as (omitting the domain indication):

$$Y^-(z) = -\frac{\tilde{J}_z(z)}{\tilde{V}(z)} \quad -\infty < z \leq z(IS), \tag{11}$$

$$Y^+(z) = \frac{\tilde{J}_z(z)}{\tilde{V}(z)} \quad z(IS) \leq z < \infty. \tag{12}$$

Through the introduction of Y^- and Y^+ in a recurrence scheme (in the next section), we can directly determine the (spectral) electric potential, uniquely, from the input admittances at the source level. The electrical potential, in turn, leads to the computation of the constants on the source level. Starting with these known constants (at the source level), the amplitudes at other interfaces would be obtained easily.

The boundary conditions

To develop the computational scheme, we introduce a possibly fictitious horizontal interface at the source level, $z(IS)$, where the point source of current injection or extraction of magnitude $I(IS)$ is located. For the given type of excitation, the electric potential is continuous across the interfaces, while the vertical component of the volume density of electric current makes a nonzero jump at the source interface. Accordingly, we have

$$\lim_{z \downarrow z(ID)} \tilde{V}(ID, z) = \lim_{z \uparrow z(ID)} \tilde{V}(ID - 1, z) \tag{13}$$

and

$$\lim_{z \downarrow z(ID)} \tilde{J}_z(ID, z) - \lim_{z \uparrow z(ID)} \tilde{J}_z(ID - 1, z) = I(ID)\delta(ID, IS), \tag{14}$$

$$\text{for } ID = 1, \ldots, IS, \ldots, ND,$$

where $\delta(ID, IS)$ is the Kronecker symbol, $\delta(ID, IS) = 1$ for $ID = IS$ and $\delta(ID, IS) = 0$ for $ID \neq IS$. Considering equations (11)–(14), we note that the admittances $Y^-(z)$ and $Y^+(z)$ are continuous across any source-free interface.

ELECTRICAL POTENTIAL AT THE SOURCE LEVEL (RECURRENCE RELATION FOR THE ELECTRIC POTENTIAL)

Using equations (5)–(8) and equation (11), we express the vertical admittances at two consecutive interfaces $z(ID)$ and $z(ID + 1)$ of any layer above and including the source level in terms of the electric potential amplitudes $A^+(ID)$ and $A^-(ID)$, viz.

$$Y^-(z(ID)) = -\lambda\sigma(ID)\frac{A^+(ID) - A^-(ID)\exp(-\lambda h(ID))}{A^+(ID) + A^-(ID)\exp(-\lambda h(ID))}, \tag{15}$$

$$Y^-(z(ID + 1)) = -\lambda\sigma(ID)\frac{A^+(ID)\exp(-\lambda h(ID)) - A^-(ID)}{A^+(ID)\exp(-\lambda h(ID)) + A^-(ID)} \tag{16}$$

$$\text{for } ID = 1, \ldots, IS - 1.$$

Here, $h(ID)$ is the thickness of the layer $D(ID)$. Besides, the admittance at any level above the uppermost interface is [cf. equations (7), (8) and (11)]

$$Y^-(z) = \lambda\sigma(0) \quad \text{for } -\infty < z < z(1). \tag{17}$$

In particular, the vertical admittance at $z(1)$ is

$$Y^-(z(1)) = \lambda\sigma(0). \tag{18}$$

In a similar manner the vertical admittance at any level $z > z(ND)$ is [cf. equations (9), (10), and (12)]

$$Y^+(z) = \lambda\sigma(ND) \quad \text{for } z(ND) < z < \infty. \tag{19}$$

In particular, the admittance at the lowermost interface $z(ND)$ is

$$Y^+(z(ND)) = \lambda\sigma(ND). \tag{20}$$

From equation (15) we obtain a relationship between the amplitudes on the interfaces enclosing a domain $D(ID)$ as

$$A^+(ID) = \Gamma^-(ID)A^-(ID)\exp(-\lambda h(ID)), \tag{21}$$

where

$$\Gamma^-(ID) = \frac{\lambda\sigma(ID) - Y^-(z(ID))}{\lambda\sigma(ID) + Y^-(z(ID))} \tag{22}$$

$$\text{for } ID = 1, \ldots, IS - 1.$$

Now, using equation (21), we express $A^+(ID)$ in terms of $A^-(ID)$ in equation (16) and obtain the following recurrence relation [via equation (22)]:

$$Y^-(z(ID + 1)) = \lambda\sigma(ID)\frac{1 - \Gamma^-(ID)\exp(-2\lambda h(ID))}{1 + \Gamma^-(ID)\exp(-2\lambda h(ID))} \tag{23}$$

$$\text{for } ID = 1, \ldots, IS - 1.$$

In a similar manner as above, using vertical input admittances at two consecutive interfaces below and including the source level,

$$Y^+(z(ID)) = \lambda\sigma(ID)\frac{A^+(ID) - A^-(ID)\exp(-\lambda h(ID))}{A^+(ID) + A^-(ID)\exp(-\lambda h(ID))}, \tag{24}$$

$$Y^+(z(ID + 1)) = \lambda\sigma(ID)\frac{A^+(ID)\exp(-\lambda h(ID)) - A^-(ID)}{A^+(ID)\exp(-\lambda h(ID)) + A^-(ID)} \tag{25}$$

$$\text{for } ID = IS, \ldots, ND - 1,$$

and starting from equation (25), we obtain

$$A^-(ID) = \Gamma^+(ID)A^+(ID)\exp(-\lambda h(ID)), \tag{26}$$

where

$$\Gamma^+(ID) = \frac{\lambda\sigma(ID) - Y^+(z(ID + 1))}{\lambda\sigma(ID) + Y^+(z(ID + 1))} \tag{27}$$

$$\text{for } ID = ND - 1, \ldots, IS,$$

and the following recurrence relation [via equation (26) and substitution in equation (24)]:

$$Y^+(z(ID)) = \lambda\sigma(ID)\frac{1 - \Gamma^+(ID)\exp(-2\lambda h(ID))}{1 + \Gamma^+(ID)\exp(-2\lambda h(ID))} \tag{28}$$

$$\text{for } ID = ND - 1, \ldots, IS.$$

Starting with the known initial values of $Y^-(z(1))$ and $Y^+(z(ND))$ given in equations (18) and (20), the recurrence relations, equations (23) and (28), are used to obtain $Y^-(z(IS))$ and $Y^+(z(IS))$ at the source level. While executing the recurrence scheme, the computed values of $\{\Gamma^-(ID); ID = 1, \ldots, IS - 1\}$ and $\{\Gamma^+(ID); \{ID = ND - 1, \ldots, IS\}$ are stored for later use in determining the electric potential spectral amplitude coefficients on the interfaces. Knowing $Y^-(z(IS))$ and $Y^+(z(IS))$ we can immediately

compute from equations (11)–(14) the (unique) electrical potential at the source level $\tilde{V}(z(IS))$ (using interface indication)

$$\tilde{V}(z(IS)) = \frac{I(IS)}{Y^-(z(IS)) + Y^+(z(IS))}. \quad (29)$$

ELECTRICAL POTENTIAL AT AN ARBITRARY DEPTH LEVEL

From equations (5), (6), and (11) for $ID = IS - 1$, we can write the field quantities at the source level as

$$\tilde{V}(z(IS)) = A^+(IS-1)\exp(-\lambda h(IS-1)) + A^-(IS-1), \quad (30)$$

$$Y^-(z(IS))\tilde{V}(z(IS)) = \lambda\sigma(IS-1)A^-(IS-1) - \lambda\sigma(IS-1)A^+(IS-1) \cdot \exp(-\lambda h(IS-1)). \quad (31)$$

Alternatively, we have for $ID = IS$ [cf. equations (5), (6), and (12)]

$$\tilde{V}(z(IS)) = A^+(IS) + A^-(IS)\exp(-\lambda h(IS)), \quad (32)$$

$$Y^+(z(IS))\tilde{V}(z(IS)) = \lambda\sigma(IS)A^+(IS) - \lambda\sigma(IS)A^-(IS)\exp(-\lambda h(IS)). \quad (33)$$

Solving equations (30) and (31) for $A^-(IS-1)$, we obtain

$$A^-(IS-1) = \tilde{V}(z(IS))\frac{\lambda\sigma(IS-1) + Y^-(z(IS))}{2\lambda\sigma(IS-1)}. \quad (34)$$

Substituting expression (29) for $\tilde{V}(z(IS))$, we find

$$A^-(IS-1) = \frac{I(IS)}{2\lambda\sigma(IS-1)}\frac{\lambda\sigma(IS-1) + Y^-(z(IS))}{Y^-(z(IS)) + Y^+(z(IS))}. \quad (35)$$

In a similar manner we solve equations (32) and (33) for $A^+(IS)$ and use equation (29) to obtain

$$A^+(IS) = \frac{I(IS)}{2\lambda\sigma(IS)}\frac{\lambda\sigma(IS) + Y^+(z(IS))}{Y^-(z(IS)) + Y^+(z(IS))}. \quad (36)$$

Once the constants $A^-(IS-1)$ and $A^+(IS)$ on the source level have been calculated, the constants on all the interfaces can be calculated straightforwardly. From the boundary condition given in equation (13), we write using equation (5)

$$A^+(ID) + A^-(ID)\exp(-\lambda h(ID)) = A^+(ID-1)\exp(-\lambda h(ID-1)) + A^-(ID-1). \quad (37)$$

We use the relationship equation (21), for substituting for the A^+ amplitudes in equation (37), and obtain

$$A^-(ID-1) = \frac{1+\Gamma^-(ID)}{1+\Gamma^-(ID-1)\exp[-2\lambda h(ID-1)]} \times A^-(ID)\exp[-\lambda h(ID)], \quad (38)$$

$$\text{for } ID = IS-1, \ldots, 1.$$

We repeat equation (21) for convenience,

$$A^+(ID) = \Gamma^-(ID)A^-(ID)\exp(-\lambda h(ID)), \quad (39)$$

$$\text{for } ID = IS-1, \ldots, 1.$$

The left-hand sides of equations (38) and (39) are the amplitudes on either side of an interface in terms of the amplitude just below it. Now, starting with the known $A^-(IS-1)$ at the source level [cf. equation (35)] we can calculate all the amplitudes on the interfaces above the source level by repeated use of equations (38) and (39). In a similar way, using equation (26) in equation (37) for index $ID+1$, we have

$$A^+(ID+1) = \frac{1+\Gamma^+(ID)}{1+\Gamma^+(ID+1)\exp[-2\lambda h(ID+1)]} \times A^+(ID)\exp[-\lambda h(ID)] \quad (40)$$

$$\text{for } ID = IS, \ldots, ND-1,$$

together with equation (26) which we repeat for convenience,

$$A^-(ID) = \Gamma^+(ID)A^+(ID)\exp(-\lambda h(ID)), \quad (41)$$

$$\text{for } ID = IS, \ldots, ND-1.$$

The left-hand sides of equations (40) and (41) are the amplitudes on either side of an interface in terms of the amplitude just above it. Now, starting with the known $A^+(IS)$ at the source level [cf. equation (36)] we can calculate all the amplitudes on the interfaces below the source level by repeated use of equations (40) and (41). Knowing the amplitudes, we use equations (3) and (5) to compute the electric potential at any point (except at the source point) in the layered earth. For the single-borehole computation for which $r = 0$ [giving $J_0(\lambda r) = 1$ in equation (3)], we use a Gauss-Laguerre quadrature method for computing equation (3). For the hole-to-hole computation of electrical potential, the method of convolution (Ghosh 1971) is used for the rapid computation of equation (3).

NUMERICAL EXAMPLES

In this section, we use the formalism presented above for the computation of the electric potential along vertical lines, because of the static electric current injection and extraction by the two point electrodes at two different depths in the layered earth models. The configuration is shown in Figure 2. Points A and B represent two electric current point electrodes at any depth along a vertical line that we will call the source line AB. CD, EF, and GH are three vertical lines at horizontal distances of 10, 30, and 50 m from AB that we will call receiver lines. A set of electrodes M and N (2 m apart) is used for the end-on-end electric potential measurements along each of the vertical lines. The measurements are converted into apparent resistivity (ρ_a), using

$$\rho_a = K\frac{\Delta V}{I}, \quad (42)$$

where ΔV is the electrical potential difference between M and N, and the geometric factor K is given by the following combination of various distances:

$$K = \frac{4\pi}{1/AM + 1/\bar{A}M - 1/AN - 1/\bar{A}N - 1/BM - 1/\bar{B}M + 1/BN + 1/\bar{B}N}. \quad (43)$$

Here, for instance, AM is the distance between A and M, and $\bar{A}M$ is the distance between the image of A with respect to the surface of the half-space and M. Similarly, we have the other distances.

To check our computer code, we considered the electric current point electrodes to be buried in layered models and assigned the same resistivity to each layer to simulate a uniform half-space model for which the exact solution is analytically known. For our computation, we have used a Gauss-Laguerre quadrature method when the electrical potentials are computed along the source line, and the convolution method using the filters given in Koefoed et al. (1972) and Anderson (1979) when the electrical potentials are computed along the receiver lines. The computed electrical potential values are in excellent agreement, up to five decimal places, with the analytical results. Moreover, we have used reciprocity as a check for our computational accuracy. However, a small error in the potential computation is amplified in the apparent resistivity values by the large geometric factor near the source level. To avoid confusion in considering the apparent resistivity curves, in Figures 3–6, we will present no apparent resistivity values near the source levels.

First, we consider the following K-type and H-type three-layer earth models:

K-type.—

$$\rho(1) = 50\ \Omega\ \text{m},\ \rho(2) = 100\ \Omega\ \text{m},\ \rho(3) = 50\ \Omega\ \text{m},$$

$$h(1) = 30\ \text{m},\ h(2) = 20\ \text{m}.$$

H-type.—

$$\rho(1) = 100\ \Omega\ \text{m},\ \rho(2) = 50\ \Omega\ \text{m},\ \rho(3) = 100\ \Omega\ \text{m},$$

$$h(1) = 30\ \text{m},\ h(2) = 20\ \text{m}.$$

In the above, we have used the resistivity ρ (inverse of conductivity) instead of the conductivity σ of a layer. This is preferred since we will present the computational results in the form of apparent resistivity. The resistivity model in a figure will be represented by a solid line. Apparent resistivities along the source line will be represented by a small-dashed line, whereas along the receiver lines at 10, 30, and 50 m, they are given by a dotted line, a dash-dotted line, and a large-dash line, respectively.

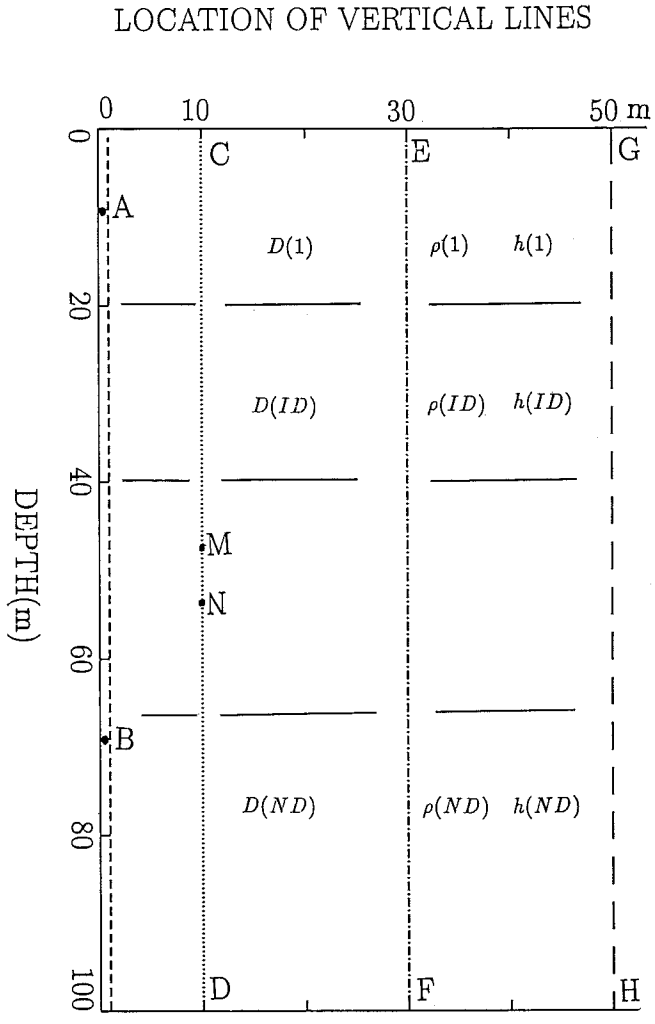

FIG. 2. Layered earth models containing the static current electrodes at A and B. Electrical potentials are measured by lowering the potential electrodes M and N (2 m apart) along the vertical lines passing through AB (source line) and CD, EF, and GH (receiver lines) at distances 10, 30, and 50 m from AB.

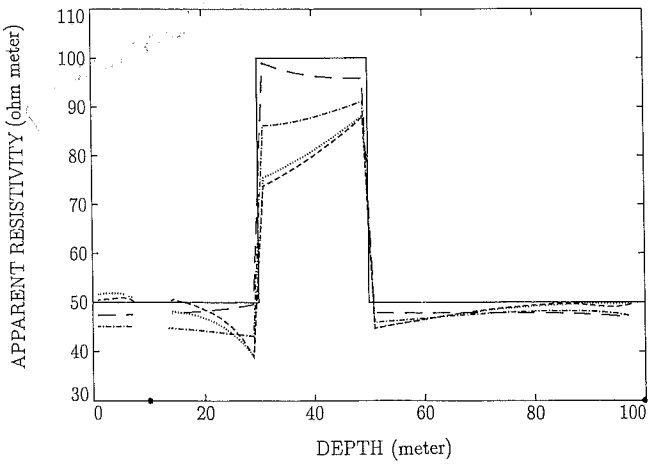

FIG. 3. Apparent resistivities along the vertical lines (i.e., the source line and the receiver lines) in the K-type earth model. Model parameters are: $\rho(1) = 50\ \Omega$ m, $\rho(2) = 100\ \Omega$ m, $\rho(3) = 50\ \Omega$ m; $h(1) = 30$ m, $h(2) = 20$ m. Electric current electrodes are located at 10 m and 100 m below the surface.

Considering the electric current electrodes A and B at depths of 10 and 100 m (represented by filled circles on the depth axis), in Figure 3 we have plotted the apparent resistivities at different depths (at the centers of MN) of the given K-type layered model. It is observed that the apparent resistivity values along the source line (simulating a single-borehole situation) and along the receiver line at 10 m converge to the resistivities of the top and bottom layers of the model away from the interfaces. In the intermediate layer, the measured profile is close to the true resistivity only in the farthest borehole at 50 m. The interfaces are clearly detected in their positions by a linear change in the apparent resistivity values in all the profiles. It may be remarked that the apparent resistivity profile in the farthest hole at 50 m is a close representation of the true distribution of the layered earth parameters (i.e., resistivities and thicknesses). Now we consider A at the surface of the earth and B at a depth of 80 m below the surface and present the computations along the vertical lines for the K-type and H-type models. The apparent resistivity profiles in Figures 4 and 5 for K-type and H-type models, respectively, follow the resistivity profile of the model. In both cases, the furthest profiles closely depict the models. Keeping the electric current electrode A at the surface and placing the electrode B at a greater depth of 100 m, we show in Figure 6 apparent resistivities for the following five-layer model:

Five-layer model.—

$$\rho(1) = 100\ \Omega\ \text{m},\ \rho(2) = 50\ \Omega\ \text{m},\ \rho(3) = 300\ \Omega\ \text{m},$$

$$\rho(4) = 20\ \Omega\ \text{m},\ \rho(5) = 500\ \Omega\ \text{m},\ h(1) = 10\ \text{m},$$

$$h(2) = 30\ \text{m},\ h(3) = 20\ \text{m},\ h(4) = 10\ \text{m}.$$

The five segments of the curves correspond to the five layers in the model, and the interfaces are located in their positions. The true resistivities of the layers are reflected in the curves. Again, the profile along the hole at 50 m is a closer representation of the resistivity and thickness distributions of the five-layer model.

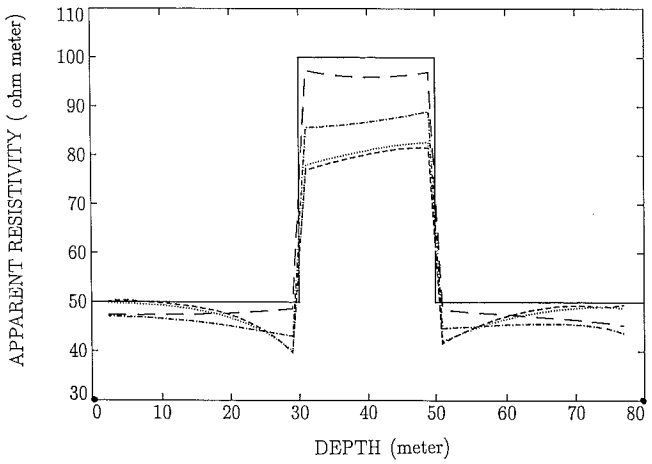

FIG. 4. Apparent resistivities along the vertical lines in the K-type earth model. Model parameters are the same as in Figure 3. Electric current electrodes are located at 0 m and 80 m below the surface.

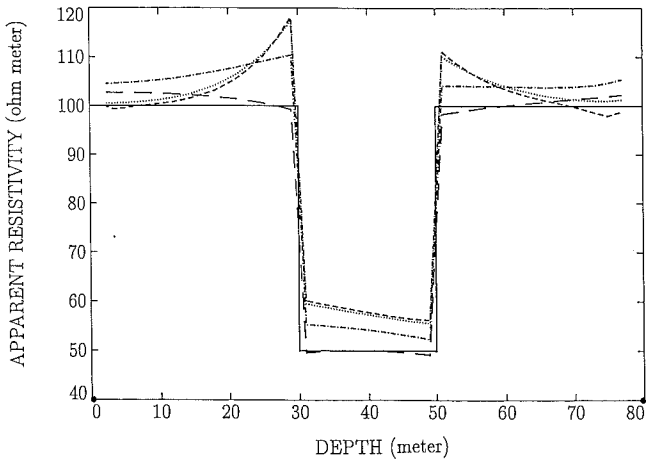

FIG. 5. Apparent resistivities along the vertical lines for the H-type earth model. Model parameters are: $\rho(1) = 100\ \Omega$ m, $\rho(2) = 50\ \Omega$ m, $\rho(3) = 100\ \Omega$ m; $h(1) = 30$ m, $h(2) = 20$ m. Electric current electrodes are located at 0 m and 80 m below the surface.

CONCLUSION

Numerical instability, which may arise in the propagator matrix formalism for computing the electric potentials because of the point electric current sources at any arbitrary depths in a layered earth, is avoided in the present spectral formalism by using only exponential functions with negative arguments. The recurrence scheme in the vertical admittance is efficient to calculate the unknown constants at the source level at an arbitrary depth. From these known constants and using the continuity relations of the potentials across the interfaces, we have derived the constants on all the interfaces for computing electric potentials at any arbi-

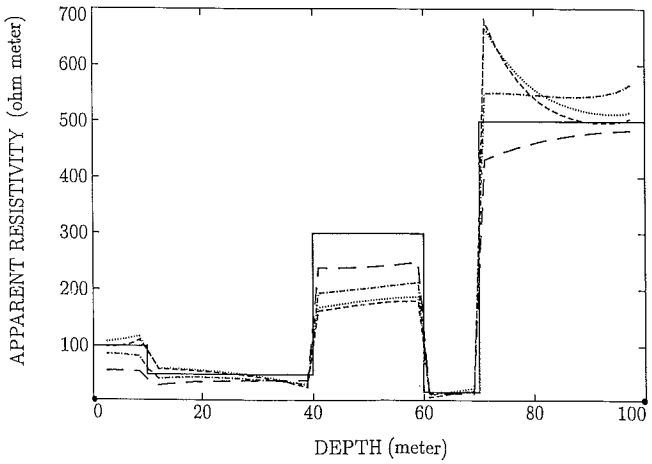

FIG. 6. Apparent resistivities along the vertical lines in the five-layer earth model. Model parameters are: $\rho(1) = 100\ \Omega$ m, $\rho(2) = 50\ \Omega$ m, $\rho(3) = 300\ \Omega$ m, $\rho(4) = 20\ \Omega$ m, $\rho(5) = 500\ \Omega$ m, $h(1) = 10$ m, $h(2) = 30$ m, $h(3) = 20$ m, $h(4) = 10$ m. Electric current electrodes are located at 0 m and 100 m below the surface.

trary depth levels. The scheme would be efficiently implemented for imaging the subsurface conductivity. The method can be similarly extended (as rightly pointed out by one of the reviewers) to other areas such as induced polarization and electromagnetic coupling.

The apparent resistivities obtained from the potential measurements reflect the true resistivity distributions of a layered earth. The numerical examples that simulate the single-borehole and the cross-borehole experiments (neglecting the borehole effects) show that injecting an electrical current at the surface of the earth and extracting the current at a large depth, with static potential measurements in adjacent boreholes, would lead to the determination of resistivities and thicknesses of a layered earth. The hole-to-hole measurements with a suitable separation between the holes may produce an apparent resistivity depth profile which may, reliably, represent the true resistivities and thicknesses of the layered earth.

ACKNOWLEDGMENTS

This paper is an outgrowth of the research supported through research funds of the Executive Board of the Delft University of Technology, The Netherlands.

REFERENCES

Anderson, W. L., 1979, Numerical integration of related Hankel transforms of orders 0 and 1 by adaptive digital filter: Geophysics, **44**, 1287–1305.

Bhattacharya, P. K., and Patra, H. P., 1968, Direct current geoelectrical sounding: Elsevier Science Publication Co.

Daniels, J. J., 1978, Interpretation of buried electrode data using a layered earth model: Geophysics, **43**, 988–1001.

Fahmy, A. H., and Alder, E. L., 1973, Acoustoelectric surface waves in multilayers, a matrix approach: Proc. 1973 Ultrason. Sym. Cat. no. 73 CHO 807-8SU, 271–274.

Ghosh, D. P., 1971, The application of linear filter theory to the direct interpretation of geoelectrical sounding measurements: Geophys. Prosp., **19**, 192–217.

Gilbert, F., and Backus, G. E., 1966, Propagator matrices in elastic wave and vibration problems: Geophysics, **31**, 326–332.

Kaufman, A. A., and Keller, G. V., 1983, Frequency and transient soundings: Elsevier Science Publication Co.

Kennett, B. L., 1974, Reflections, waves and reverberation: Bull. Seis. Soc. Am., **65**, 1643–1651.

Koefoed, O., 1979, Geosounding principles 1, Resistivity sounding measurements: Elsevier Science Publication Co.

Koefoed, O., Ghosh, D. P., and Ploman, G. J., 1972, Computation of type curves for electromagnetic depth sounding with a horizontal transmitting coil by means of a digital linear filter: Geophys. Prosp., **20**, 406–420.